Ecological Indicators 146 (2023) 109816

Contents lists available at ScienceDirect

Ecological Indicators

journal homepage: www.elsevier.com/locate/ecolind

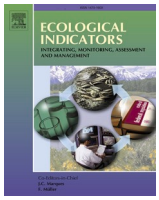

Original Articles

Emerging signals of coastal system changes under rapid anthropogenic disturbance in Hangzhou Bay, China

Chao Fan [a,b,c,d], Xiyong Hou [a,c,d,*], Qian Zheng [a,c,d], He Xu [a,b,c,d], Dong Li [a,c,d], Sandra Donnici [e], Cheng Tang [a,c,d]

[a] Yantai Institute of Coastal Zone Research, Chinese Academy of Sciences, Yantai Shandong 264003, China
[b] University of Chinese Academy of Sciences, Beijing 100049, China
[c] CAS Key Laboratory of Coastal Environmental Processes and Ecological Remediation, Yantai Institute of Coastal Zone Research, Chinese Academy of Sciences, Yantai Shandong 264003, China
[d] Shandong Key Laboratory of Coastal Environmental Processes, Yantai Shandong 264003, China
[e] National Research Council, Institute of Geosciences and Earth Resources, Via Gradenigo, 6, 35131 Padova, Italy

ARTICLE INFO

Keywords:
Coastal system
DPSR framework
Environmental indicators
Hangzhou Bay
Morphological changes
Rapid anthropogenic disturbance

ABSTRACT

Coastal systems are continuously reshaped by rapid anthropogenic disturbance globally. However, the awareness of how coastal systems adapt to rapid anthropogenic disturbance remains inadequate. Thus, this study assessed the spatial response of coastal systems to rapid anthropogenic disturbances, and a typical coastal system (Hangzhou Bay) was selected for a case study. Three environmental indicators (i.e., coastline change rate, accretion/erosion grade, and the displacement of the center of gravity) were selected to measure the morphological changes in the coastal system between 1990 and 2020. The results showed that the coastal waters of Hangzhou Bay decreased by 432 km^2, and the coastal morphology became structured driven by increasing artificial coastlines. Moreover, the accretion–erosion equilibrium of underwater elevation transitioned northwest, which derived the shift of geometric center of gravity toward the northwestern part of the coast. These fluctuating signals provided us with a macroscopic perception of coastal system changes, which is expected to provide local decision-makers with sites where coastal systems are adaption loss to assist coastal protection.

1. Introduction

Coasts are important transition zones from land to marine ecosystems (Golla et al., 2020; Hopper et al., 2021). Globally, coastal systems are among the most valuable and vulnerable ecosystems (Hossain et al., 2020; Kron, 2013). They prevent exposures to natural hazards (e.g., coastal flooding and tsunamis) by buffering storm surges (Loder et al., 2009; Tognin et al., 2021), increasing carbon sinks (Lovelock and Reef, 2020; Ward et al., 2021), balancing sediment and nutrient cycling (Lonborg et al., 2021; McLachlan et al., 2020), and constituting sanctuaries for biodiversity (Hopper et al., 2021; Pereira et al., 2021). However, despite the benefits that people derive from coastal systems, rapid anthropogenic disturbances[1] pose environmental pressure on coasts (Bolivar et al., 2019; Carranza et al., 2020; Fan et al., 2018). Important examples include reclamation projects that increasingly invade coastal wetlands (Qiu et al., 2021; Wang et al., 2010). Therefore, a rising concern is whether such changes will substantially affect coastal resilience to adapt to global changes (Cooper et al., 2020; Wang et al., 2020a).

Far less understood is how coastal systems respond to rapid anthropogenic disturbances (Foley et al., 2017; Singh et al., 2017; Williams et al., 2022). In China, coastal construction projects have contributed cumulative impacts to coastal surroundings, which have dramatically threatened the regular succession of coastal systems (Hou et al., 2017; Xu et al., 2017; Yi et al., 2018; Zhou et al., 2018). However, project impact assessments for coastal environments are often limited to

* Corresponding author at: Yantai Institute of Coastal Zone Research, Chinese Academy of Sciences, Yantai Shandong 264003, China.
E-mail address: xyhou@yic.ac.cn (X. Hou).

[1] Anthropogenic disturbances (fast variable) often cause stronger impacts on coastal systems than natural factors (slow variable, e.g., sea level rise). Coastal ecosystems are naturally exposed to recurrent disturbances, which act as drivers of ecosystem dynamics. However, in recent decades, rapid anthropogenic disturbance has exerted intense pressures, resulting in altered dynamics and thus, reduced resilience. The rapid anthropogenic disturbance in HZB often points to the coastal construction projects, such as reclamation, whose construction stage is usually between months to several years (Table S7).

https://doi.org/10.1016/j.ecolind.2022.109816
Received 6 October 2022; Received in revised form 17 November 2022; Accepted 14 December 2022
Available online 19 December 2022

small buffering areas adjacent to project locations, and the temporal scales of these assessments are short (Wang and Zhang, 2022). Hence, the significant conflicts lay between real project impacts on surroundings and inadequate assessments (individual project-based assessments) in a long-term perspective. This conflict may prevent stakeholders (e.g., residents and governments) from clearly understanding how coastal systems respond to rapid anthropogenic disturbance.

Morphological changes are key indicators visually reflecting the response of coastal systems to rapid anthropogenic disturbance in macroscopic scales (Aiello et al., 2013; Bolla Pittaluga et al., 2015; Thomas et al., 2002; Zhang et al., 2015). Hotspots of morphological changes are often located where coastal system have been exposed to rapid anthropogenic disturbance (Grases et al., 2020). Morphological sharply changes indicate that coastal systems adapt to human disturbance through the transition of stable states into new niches (Beisner et al., 2003; Rietkerk et al., 2021; Wang et al., 2013). Therefore, monitoring coastal morphological succession is expected to verify whether coastal systems are resilient in adapting to rapid anthropogenic disturbance (Martinez et al., 2017; Moussa et al., 2019). Nevertheless, a single geographical indicator (e.g., coastline change rate) may only measure the change in coastal morphology in inshore waters, which fails to reveal morphological change underwater.

This study thus aimed to assess the spatial response of coastal systems to rapid anthropogenic disturbance using multiple indicators. Coastal components have been identified and grouped into three broad geographic parameters (i.e., coastline, underwater elevation, and geometric center of gravity). These parameters were measured using corresponding indicators (i.e., coastline change rate, accretion/erosion grades, and the displacement of the center of gravity, respectively). Instead of instantaneous fluctuation (e.g., inundation area fluctuation driven by instantaneous tides), coastal systems changes refer to the transition of the stable states of coastal morphology.

Hangzhou Bay (HZB) is an excellent case study where coastal morphology reshaped by rapid anthropogenic disturbance (Li et al., 2018). Here through observations and assessments, we found that HZB has lost 432 km^2 of adjacent coastal waters, and the artificial coastlines increase has caused the coastal morphology to become structured. Moreover, the accretion–erosion equilibrium of underwater elevation transitioned northwest. Therefore, coastal morphological changes have driven the transition of the geometric center of gravity toward the northwest. The resultant signals of the morphological changes in HZB are expected to provide early warning signals for coastal management to promote sustainable coastal development.

2. Materials and methodology

2.1. Study area

HZB, spanning 90 km across the east–west direction and covering an area of about 4,800 km^2, is a typical funnel-shaped tide-dominated estuary of the Qiantang River (Wang and Eisma, 1990; Xie et al., 2017). Its northern part features plain and multiple submarine trenches, whereas the south is plain at high latitudes but hilly at low latitudes (Fig. 1).

Moreover, HZB has a subtropical monsoon climate. The mean temperature is 17 °C, and the precipitation is concentrated between April to September, with an annual mean rainfall of 1600 mm (Xie et al., 2017). Additionally, a semidiurnal tide with a maximum tidal current of 3.0 m/s drives the horizontal water flow into HZB, whereas the northern part is dominated by flood currents (Pan and Huang, 2010; Shao et al., 2020; Xie et al., 2013).

Urban sprawls have sharply invaded the cultivated land in HZB (Li et al., 2018), which contradicts the policy of protecting cultivated lands proposed by the central government of China (Lu et al., 2013). Thus, reclamation projects have been implemented along the coasts to gain new cultivated land to achieve such conservation goals (Li et al., 2018). Consequently, reclamation squeezed the adjacent coastal waters, which caused regional environmental quality degeneration (Qiu et al., 2021; Tian et al., 2021).

2.2. Materials and preprocessing

The materials used in this study include Landsat satellite images with

Fig. 1. Location of the study areas. The cities along the HZB belong to Zhejiang and Shanghai. (a) Landsat satellite image (2020) composed of bands 6–5-3. The northern part of the coast ranges from Haiyan to the Luchao Port (Pudong). The southern part ranges from Shangyu to the estuary of the Yongjiang River (Zhenhai); The width across is 100 km at the outer estuary and 20 km at the upper estuary. (b) Location of HZB. (c,d) Field photos of the Luchao Port and the Sea-Crossing Bridge of Zhoushan.

a spatial resolution of 30 m, bathymetric charts (Fig. 2), and land covers data. Landsat satellite images were used to monitor the coastline, and bathymetric charts were used to observe the underwater elevation (water depth). Using these data, we produced a geodatabase containing the spatial distribution of the coastline and the underwater digital elevation model (DEM). Moreover, land cover data were collected for analyzing the assessment of driving factors of coastal system changes.

2.2.1. Determining the coastline from Landsat images

The shifting locations of coastlines provide us with a macroscopic view of the morphological changes of coasts between land and sea (Zhu et al., 2014). Remote sensing images with time series enable monitoring coastline changes from a long-term perspective (Hou et al., 2016). There are three steps for monitoring coastline changes. First, atmospheric correction was implemented using the FLASH module to enhance image quality, and geometric correction was implemented using ground control points (point source: Google Earth images). Second, coastline locations were marked in the satellite images, and coastline classifications were operated based on classification criteria. Finally, guided by the classification criteria, coastline mapping was achieved using a visual interpretation method in ArcGIS 10.5. Note that the visual interpretation required the same scale for all satellite images to ensure data comparability (Su et al., 2011). Based on validation points from Google Earth images and GPS, precision evaluation was implemented using root mean square error model (RMSE), to measure the position offset of coastline, as shown in Table S6.

2.2.2. Building underwater DEM based on bathymetric charts

The underwater elevations recorded in bathymetric charts are expected to build DEM (Van der Wal and Pye, 2003). There are four steps to assess underwater elevation changes. First, bathymetric charts were defined as a unified spatial coordinate system in ArcGIS 10.5. Second, the water depth points were obtained from bathymetric charts through visual interpretation. Moreover, based on the water depth points, the underwater DEM was produced using the inverse distance weighting method in ArcGIS 10.5. Finally, the pixel-based subtraction of DEM was operated to measure changes in the water depth using a raster calculator in ArcGIS 10.5.

2.3. Methodology

The components of coastal systems (i.e., coastline, underwater elevation, and the geometric center of gravity) were quantified using three indicators (i.e., coastline change rate, accretion/erosion grades, and the displacement of the center of gravity, respectively). Therefore, these indicators were bridge tools for assessing the spatial response of coastal systems to rapid anthropogenic disturbance.

2.3.1. Calculating the coastline change rate

Coastline changes drive spatial conversion between land and sea (Hou et al., 2016; Zhu et al., 2014), which can directly inspire us with hotspots of the morphological changes on coasts. The coastline change rate represents an important indicator for measuring the morphological changes of coastal systems. The Digital Shoreline Analysis System (DSAS), an add-in to ArcGIS, provides an automated method for calculating rate-of-change statistics from multiple historical coastline positions (USGS, 2018). This indicator was calculated using DSAS, as shown in equation (1).

$$E_{i,j} = \frac{d_j - d_i}{\Delta Y_{j,i}} \tag{1}$$

where i is the intersection point of coastline and section line in initial year, j is that in end year, d_i represents the distance between coastline and baseline in initial year, d_j is that in end year, and Δy (j, i) means the time interval in the whole study periods.

2.3.2. Grade division of the accretion and erosion

Sediment accretion and erosion reshape coastal morphologies. In this study, the pixel-based subtraction of the DEM was implemented to measure underwater elevation changes, which subsequently can be divided into seven grades (Table 1) (Song et al., 2018).

2.3.3. Measurement of the geometric center of gravity

The standard deviational ellipse, SED, is a statistical method for measuring the concentration of unit locations on a map (Lefever, 1926; Wang et al., 2015). The geometric center of gravity, GCG, in an ellipse is in the concentration location of spatial object (Liu et al., 2022; Ni and Chen, 2022), and shifts of GCG imply the spatial object have suffered stability changes (i.e., morphological changes) on the entire situation. SDE tool in ArcGIS 10.5 enables the mapping of the spatial object into a mathematical coordinate system to detect the GCG (Gong, 2002). At least two GCG should be detected before measurement for the displacement of the GCG (Manhattan distance between two GCG).

In this study, coastlines of four periods, i.e., 1990, 2000, 2010 and 2020, are input data of HZB to reflect the coastal systems. In addition to coastlines of HZB, the water depths were assigned as weight to calculated GCG in 1990 and 2020. Thus, output result of GCG here has been considered both of coastline changes and underwater elevation changes. Note that Ellipse Size is a key input variable and a larger percentage value represents a bigger data covering by Ellipse. In this study, one standard derivation was chosen as an input variable for Ellipse Size. Overall, the morphological changes of coastal systems can be measured using the displacement of the GCG, as shown in equations (2)-(4).

$$\overline{X_w} = \frac{\sum_{i=1}^{n} w_i \bullet x_i}{\sum_{i=1}^{n} w_i} \tag{2}$$

$$\overline{Y_w} = \frac{\sum_{i=1}^{n} w_i \bullet y_i}{\sum_{i=1}^{n} w_i} \tag{3}$$

$$L_{ij} = \sqrt{\left(x_{wi} - x_{wj}\right)^2 + \left(y_{wi} - y_{wj}\right)^2} \tag{4}$$

where (x_i, y_i) is the spatial coordinate system for the geographic objects, w_i refers to the weight, ($\overline{Xw}$, $\overline{Yw}$) is the center of the weighted average, and L_{ij} is the displacement between i th and j th GCG of coastal systems.

3. Results

3.1. Morphological changes of coastline of the HZB

The total length of the coastline in HZB increased from 259.82 km in 1990 to 316.02 km in 2020 (Table 2). The seaward expansion rate of the coastline peaked in the first decade of 2000, with a mean rate of 3.78 km/yr. A representative hotspot of seaward expansion is in the Cixi City (Fig. 3). Noticeably, the monotonic decline trend was displayed in the standard deviation (std.) values of the coastline changes during the study periods (Table 2).

The proportion of natural coastline in HZB decreased from 78.94 % to 4.87 % (the length decreased by 224.52 km). In contrast, the total length of the artificial coastline increased from 64.43 km in 1990 to 330.44 km in 2020. Noticeably, the functions of the artificial coastline tended to diversify. In addition to tidal barriers and aquaculture dikes, three coastline functions emerged since 1990 (i.e., transport dike, reclamation, and spur dike and wharf). The most significant increase in length among those of the artificial coastline structures was that for tidal barriers.

3.2. Underwater elevation changes of the HZB

The underwater elevation in HZB increased in the upper estuary but decreased in the outer estuary (Fig. 4a, 4b). Interestingly, accretion was

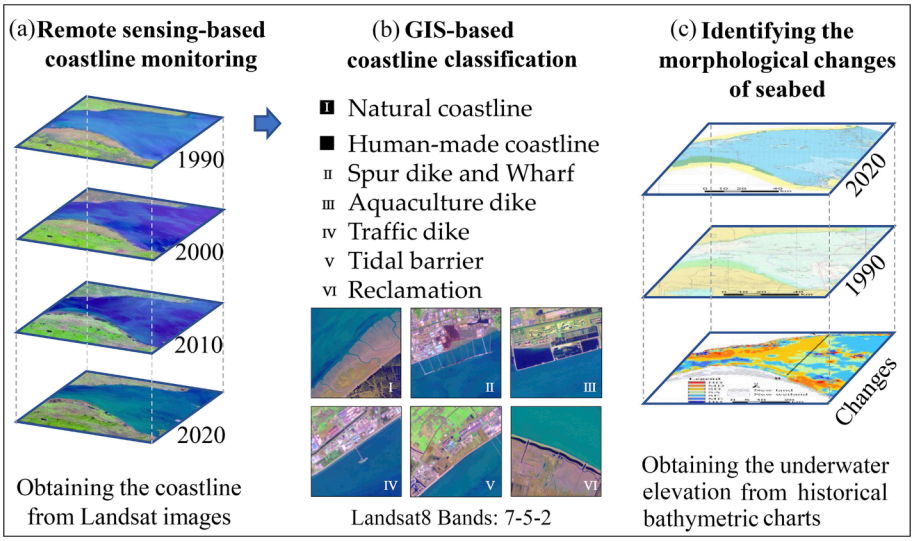

Fig. 2. Data used in this study. (a) Four remote sensing images were selected to monitor coastline changes, and the information introduction of these images have been separately uploaded in the supplementary material (Table S1-S4 and S6, and Fig. S1-S3). (b) We put forward a criterion for coastline classification (details in Table S5). (c) Bathymetric charts for building large-scale underwater DEM.[1] source: four Landsat-series satellite images were downloaded from website of United States Geological Survey: https://earthexplorer.usgs.gov/. A paper map published by China Navigation Assurance Agency (1: 25,000) and a digital map released online: https://www.shipxy.com.

Table 1
Standard for grade division of accretion and erosion.

Change trend	Interval (d/m)	Grade division	Abbreviation
Accretion	$DC \geq 5.00$	High deposition	HD
	$2.50 \leq DC < 5.00$	Moderate deposition	MD
	$0.25 \leq DC < 2.50$	Slight deposition	SD
Stable area	$-0.25 \leq DC < 0.25$	Stable area	SA
Erosion	$-2.50 \leq DC < -0.25$	Slight erosion	SE
	$-5.00 \leq DC < -2.50$	Moderate erosion	ME
	$DC < -5.00$	High erosion	HE

Note: DC refers to water depth changes, and all water depth are negative values in this study.

Table 2
Statistics of the coastline in Hangzhou Bay between 1990 and 2020.

Years	Length (km)	Change in length (km)	Std.	Proportion of the natural coastline (%)
1990	259.82	—	8.72	78.94
2000	272.00	12.17	5.61	41.05
2010	309.82	37.82	3.31	15.32
2020	316.02	6.20	2.71	4.87

Note: Std. reflects the dispersion degree of hotspots regarding coastline changes. Large std. values represent big dispersion degrees of hotspots.

slightly greater than erosion (Fig. 4c), and the morphological underwater pattern displays accretion in the west and erosion in the east. The erosion–accretion equilibrium was in the line between Fengxian and Cixi (Fig. 4c).

We observed a change pattern of northward erosion and southward accretion at the east of the equilibrium line (outer estuary). The riverbed with moderate erosion was concentrated between Fengxian and Pudong (north of the coast). Meanwhile, the riverbed with moderate accretion was concentrated between Cixi and Zhenhai (south of the coast). Inversely, there was a change pattern of northward accretion and southward erosion at the west of the equilibrium line (upper estuary). The most typical accretion area was in Jiaxing Port, where the water depth increased from − 41.60 m in 1990 to − 32.96 m in 2020 (Fig. 4a, 4b). Meanwhile, moderate erosion occurred in the south along the coast between Yuyao and Cixi.

3.3. The geometric center of gravity transition of the HZB

The geometric center of gravity (two-dimensional, 2D) in HZB transitioned toward the northeast by 2.84 km during the study period (Fig. 5). A typical period of these changes emerged in the first decade of 2000. During this period, the geometric center of gravity (2D) transitioned toward the northwest by 14.19 km. Moreover, the geometric center of gravity (three-dimensional, 3D) shifted toward the northwest by 1.35 km.

4. Discussion

4.1. Nexus between rapid anthropogenic disturbances and coastal system changes

Reclamation had a positive relationship with the seaward increase of the coastline, which rapidly squeezed adjacent coastal waters (Fig. 6a, 6b). Moreover, influenced by coastal defense projects, coastal sediment changes reshaped the underwater elevation (Xie et al., 2017). A driving–pressure–state–response (DPSR) framework was introduced for interpreting the nexus between rapid anthropogenic disturbances and the response of the coastal system to disturbances (Fig. 6c).

4.1.1. Reclamation squeezes adjacent coastal waters

High-density construction in HZB contradicts farmland conservation. The land demand for construction on coasts has sharply increased since 2008[2] (Wang and Zhang, 2022). Under economic considerations,[3] local governments (land suppliers) are willing to supply land for real estate companies to increase fiscal income (Liu, 2018; Wang et al., 2020b; Wu, 2022; Yuan et al., 2019). Thus, cultivated lands are mainly converted into construction land to support urban construction (Hu et al., 2021). Such a change in land-use patterns contradicts China's cultivated land protection policy. Because, local governments are required to abide by strict conservation targets to protect cultivated land (a goal to protect 1.8 billion mu of China's cultivated land) (Wang et al., 2020b).

Reclamation thus mitigates the risk of breaking cultivated land-protected policies. A noticeable evidence is that reclamation has increased cultivated land areas by 460.67 km^2 for the coastal HZB between 1985 and 2015 (Li et al., 2018). However, reclamation drives seaward coastline conversion, which squeezes adjacent coastal waters

[2] The 4-trillion (RMB) plan proposed by the Chinese Central Government in 2008 stimulated infrastructure construction. Construction projects in HZB have been listed in the Table S7.

[3] The land reserve system is an important fiscal source for local governments in China.

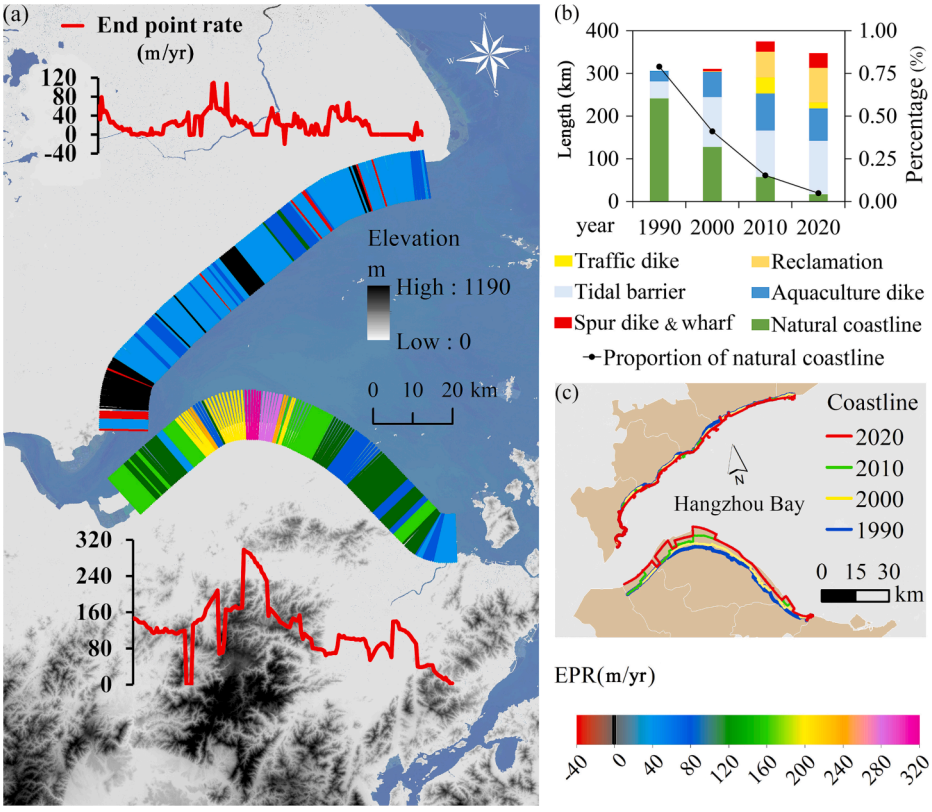

Fig. 3. Coastline changes in HZB. (a) Coastline change rate along the coasts (The X coordinate axes of end point rate is the series number of vertical lines (0–229 in north coast and 0–200 in south coast). These vertical lines with 500 m-interval connect the coastline endpoints for 1990 and 2020. Each vertical line produces an EPR value, which has been mapped into Y coordinate axes. Values of end point rate are visually presented using red curves, and the color bar link to the EPR values of vertical lines along coasts). (b) Statistics of the coastline length. (c) Distribution of the coastline in four periods. (For interpretation of the references to color in this figure legend, the reader is referred to the web version of this article.)

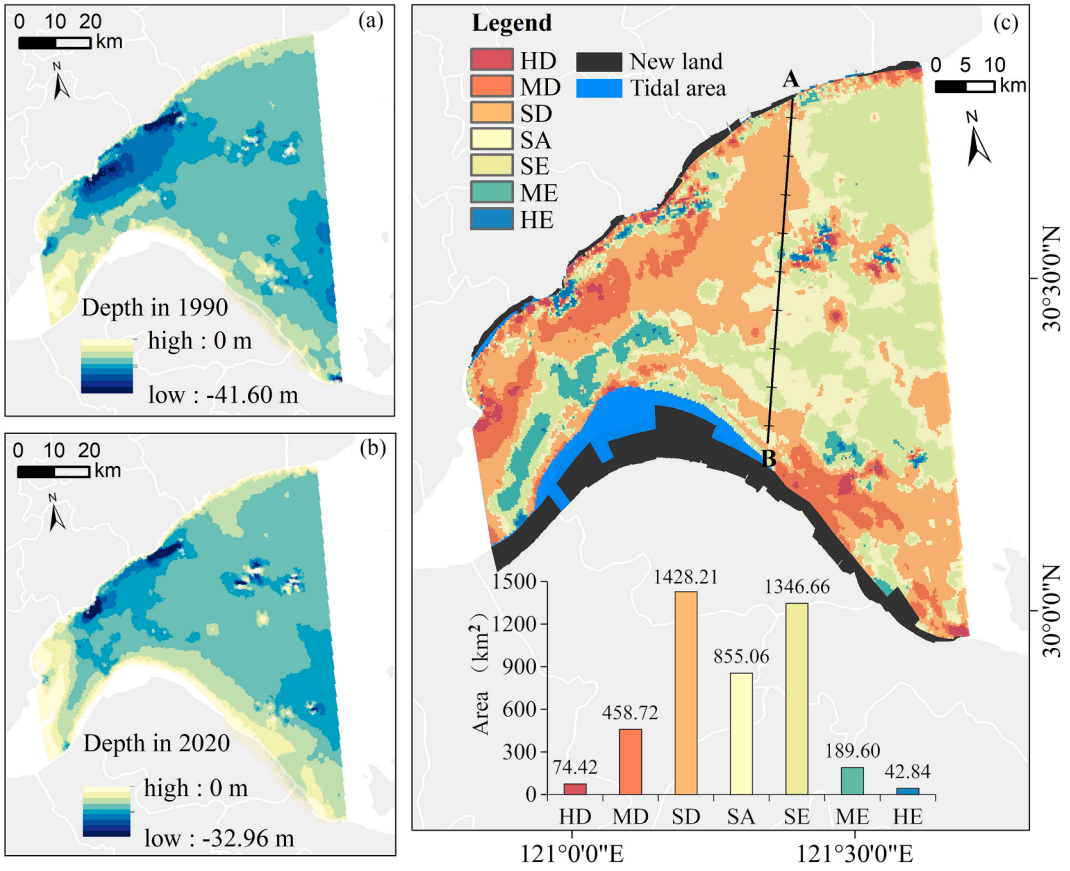

Fig. 4. Spatial pattern of the underwater elevation changes in HZB. (a)-(b) Water depth (underwater elevation) distribution in 1990 and 2020, respectively. (c) Grades of underwater elevation changes between 1990 and 2020, where the line between A and B was in the stable areas of underwater elevation.

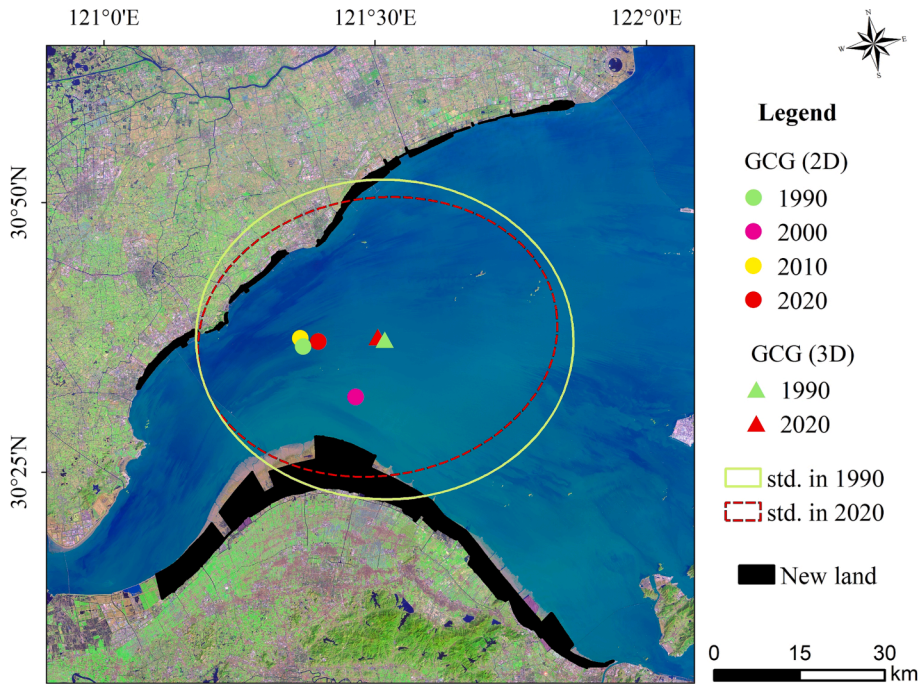

Fig. 5. Spatial distribution of the geometric center of gravity (GCG) in HZB. The background picture is Landsat satellite image (2020) in bands of 7-5-2.

(Li et al., 2018), and the coastal morphology becomes structured (The morphology of the artificial coastlines is often regular and straight) (Li et al., 2018; Tian et al., 2021; Xu et al., 2022). Coastal morphological changes then drive the GCG shifting toward the northeast by 2.84 km (Fig. 5).

To sum up, cultivated land gains come at the cost of squeezing adjacent coastal waters and natural coastline loss, which drives coastal morphology to become more regular and straight.

4.1.2. *Coastal defense projects reshape the underwater elevation*

Although the processes of coastal sediment balance usually are mediated by important feedback between sediment production and geomorphology, the key component to both lateral and vertical accretion/erosion dynamics points to sediment supply from upland and oceanic sources, which are mainly driven by fluvial delivery and tidal currents (Fan et al., 2014; Green and Coco, 2014; Hu et al., 2019; Wang et al., 2004; Xie et al., 2013). All sediments from the Qiantang River and suspended sediments at 27 % from the Yangtze River sink in the HZB (Liu, 2018; Wang et al., 2004). The path of fluvial delivery (sediment source: Qiantang River) is from the upper estuary to the outer estuary. Inversely, the path of tidal current delivery (sediment source: Yangtze River) is from the outer estuary to the upper estuary (Song et al., 2020). At the climax, most sediments sink in the north of the coast; while they sink in the south of the coast at low tide (Dai et al., 2014; Song et al., 2020). Therefore, the environmental background of the underwater elevation in HZB is mediated by sediment sources and transport paths.

Coastal defense projects reshape the underwater elevation of HZB. Coastal defense projects (e.g., embankments) could protect coastal infrastructure by lowering sediment supply to coasts (Xie et al., 2017). This solution prevents coasts from exposure to storm surges, which reinforces the safety of infrastructure along the coasts (Fig. 6b)[4] (Ariffin et al., 2018; Koraim et al., 2014). However, the increasing number of coastal defense projects calls the stability of coastal environments into question, with their lateral and vertical erosion mechanisms under threat (Bulleri and Chapman, 2010; Salmon and Duvat, 2018; Tak et al., 2020). For example, high-intensity embankments accelerated the tidal currents speed in the south of the coast, which increased the underwater elevation loss (Pan et al., 2019). Similarly, our observation proved that moderate underwater erosion occurred in Luchao Port (Fig. 4c) because the path of sediment delivery by tidal currents was hindered by embankments (artificial peninsula projects). In fact, this change shaped a westward process of sediment balance in the north of the coast (the stable area shifting from the Luchao Port to Jinshan) (Dai et al., 2014). Our monitoring confirmed that HZB has shown an overall erosion in the outer estuary, and the geometric center of gravity (3D) has moved toward the upper estuary by 1.35 km.

In summary, coastal defense projects alter sediment fluxes and transport pathways, which is an important factor in the reshaping of the underwater elevation in the HZB.

4.2. *Priority sites to assist natural coastline restoration*

Natural coastline restoration in HZB is urgently needed. The proportion of natural coastline in HZB fail to meet the protected proportion proposed by Chinese Centre Government[5] (PGGP, 2019). Results in Table 2 show that the proportion of natural coastline in HZB decreases from 78.94 % in 1990 to 4.87 % in 2020, which is the most significant signal of coastal systems changes in this study. Given local governments in China are required to strictly abide the coastline protection goals, restoration of natural coastlines is expected to be the viable solution to achieve protection goals in future.

Where are the priority sites for natural coastline restoration is a critical problem for local governments. Because local governments need to consider the benefit conflict between natural coastline protection and economic cost. Our results show that artificial coastlines (e.g., tidal barrier and traffic coastlines) in HZB colonized majority of the sites

[4] Reclamation in coastal China has been forbidden to protect coastal wetland since 2018. Regulation by this policy, many reclamation regions are converted to the construction land, and become urban hotspots, as shown in increasing spatial overlapping between urban area and reclamation land. But these areas are early aimed to balance the total number of the cultivated land.

[5] Proportion of natural coastline should be larger than 12 % in Shanghai and 35 % in Zhejiang, respectively.

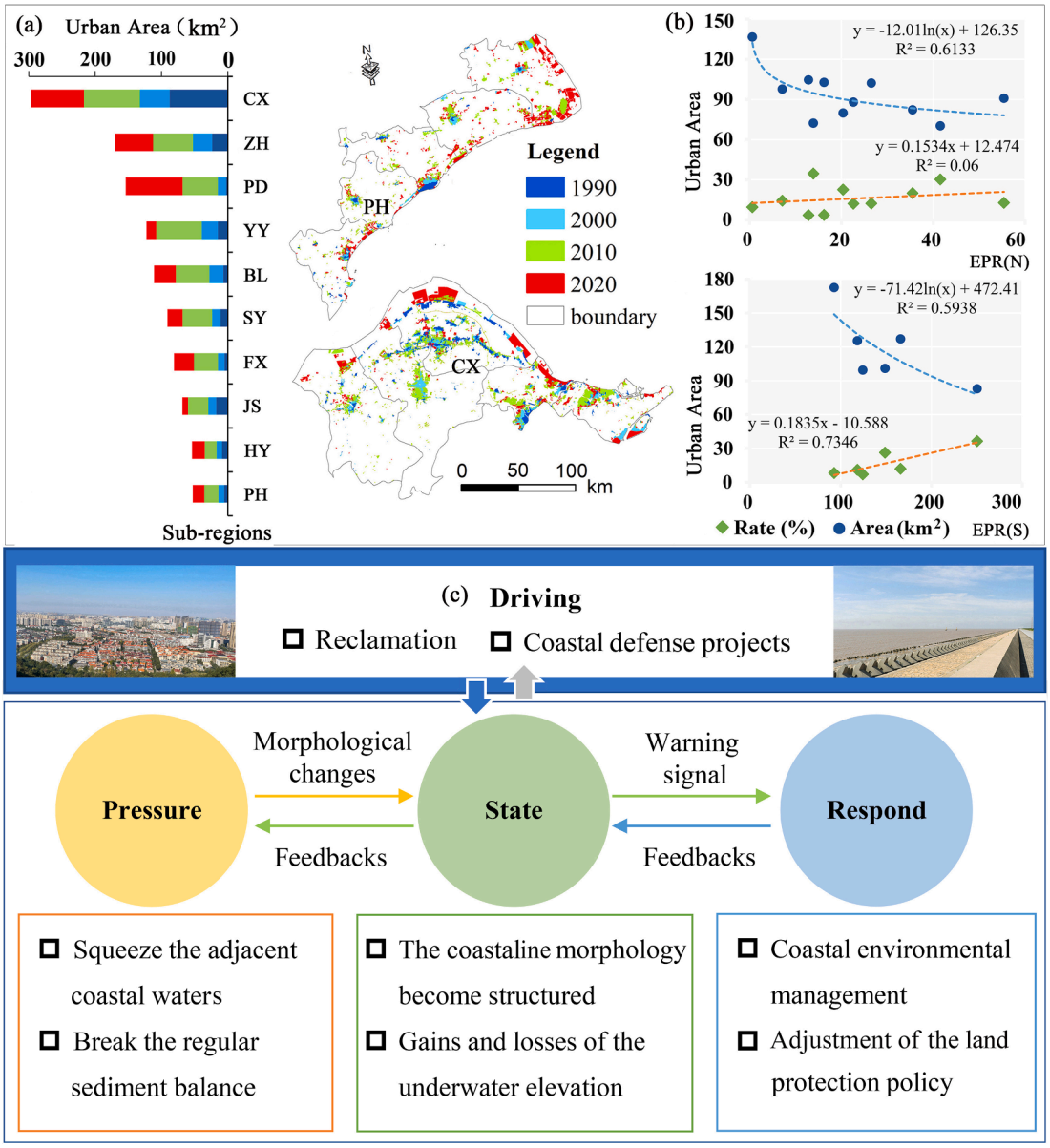

Fig. 6. A DPSR framework used to interpret our analysis of the spatial response of coastal systems to rapid anthropogenic disturbance. (a) The urban area (impervious surfaces) increased by 6.53 times between 1990 and 2020 (10 km inner upland along the coastline). Source of land-use data: Resource Environment Center of Chinese Academy of Sciences. (b) Spatial correlation between coastline change rate and urban distribution (sampling based on fishnet with a resolution of 10 × 10 km). (c) Nexus among urban sprawl, pressure on coasts, the response of coastal morphology, and coastal management. Moreover, the abbreviations (i.e., CX, ZH, PD, YY, BL, SY, FX, JS, HY, and PH) respectively are Ci Xi, Zhenhai, Pudong, Yuyao, Beilun, Shangyu, Fengxian, Jinshan, Haiyan, and Pinhu.

where call for improving economic benefits, and removing artificial coastlines often fail to represent an economic-friendly solution. China's ecological economists advocate to recover the ecological functions of coastlines rather than remove the artificial coastlines (Jia et al., 2019). In this context, establishment of new siltation environment should be a prior consideration rather than redraw the natural coastlines to their initial sites. In other words, the restoration sites are expected to be located outside the artificial coastline.

This study is expected to inform the decision-makers with the spatial information regarding the sites where coasts (artificial coastlines) are adjacent to good siltation environments (Fig. 4c). These sites can be planned to give priority to assist natural coastline restoration. Coasts adjacent to Cixi City where is abundant in sediment sink have potential to be a perfect site for natural coastline restoration (e.g., muddy coastline and sand coastline).

4.3. Strength and weakness in this study

From a macroscopic scale, this study revealed the spatial response of the coastal system to rapid human disturbance. These disturbances point to cumulative human impacts rather than individual one on coastal system. Hotspots of coastal system changes have been efficiently monitored, and the resultant data is expected to assist environmental planning and management regarding natural coastline restoration. Moreover, based on field data, criteria for coastline classification in different geomorphologic sites and corresponding interpretation standards on remote sensing images were established.

However, coastline extraction technology in this study highly relies on expert knowledge. While expert knowledge is viable to distinguish most coastline types in landsat images, there is still some confusion regarding the precise identification of traffic dike and tidal barrier. Because these coastlines have similar morphologic characteristics in

landsat images. Thus, it is necessary to check the accuracy of coastline via abundant filed data and high-resolution images (e.g., Google Earth images).

5. Conclusion

This study assessed how coastal systems adapt to rapid anthropogenic disturbance using three indicators (i.e., coastline change rate, accretion–erosion grade, and the displacement of GCG), and a typical coastal system (HZB) was selected as a case study. Through observations and assessments of the HZB, we found that the adjacent coastal waters of HZB decreased by 432 km^2, and the coastal morphology became structured, because the natural coastline was replaced by artificial coastline by 74.07 %. Noticeably, the accretion–erosion equilibrium transitioned northwest of the coasts, which drive the geometric center of gravity shifting toward the northwestern part of the coasts. These fluctuating signals provided us with a macroscopic perception of coastal system changes. Moreover, we discussed the nexus between anthropogenic disturbances and the coastal systems, and discussed the potential values of our results in assisting natural coastline restoration.

CRediT authorship contribution statement

Chao Fan: Conceptualization, Methodology, Software, Validation, Formal analysis, Data curation, Writing – original draft, Writing – review & editing, Visualization. **Xiyong Hou:** Funding acquisition. **Qian Zheng:** Methodology, Validation. **He Xu:** Validation. **Dong Li:** Writing – original draft, Writing – review & editing. **Sandra Donnici:** Funding acquisition. **Cheng Tang:** Funding acquisition.

Declaration of Competing Interest

The authors declare that they have no known competing financial interests or personal relationships that could have appeared to influence the work reported in this paper.

Data availability

Data will be made available on request.

Acknowledgments

We would like to thank Professor Feng Gui (Zhejiang Ocean University), and Wangyuan Zhu (Zhejiang Ocean University) for providing us with bathymetric charts. Moreover, we would like to thank for the comments from Yuxin Zhang (CAS, Yantai Institute of Coastal Zone Research), editors and peer reviewers.

Funding

This work was supported by the Strategic Priority Research Program of the Chinese Academy of Sciences, Grant No. XDA19060205; The National Natural Science Foundation of China (grant No. 42176221); And the 2020-2022 Scientific Cooperation Program between the National Research Council of Italy and the Chinese Academy of Sciences, Project “Coastal system changes over the Anthropocene: Natural Vs Induced drivers”.

Appendix A. Supplementary data

Supplementary data to this article can be found online at https://doi.org/10.1016/j.ecolind.2022.109816.

References

Aiello, A., Canora, F., Pasquariello, G., Spilotro, G., 2013. Shoreline variations and coastal dynamics: A space-time data analysis of the Jonian littoral, Italy. Estuar. Coast. Shelf Sci. 129, 124–135.
Ariffin, E.H., Sedrati, M., Akhir, M.F., Daud, N.R., Yaacob, R., Husain, M.L., 2018. Beach morphodynamics and evolution of monsoon-dominated coasts in Kuala Terengganu, Malaysia: Perspectives for integrated management. Ocean Coast. Manag. 163, 498–514.
Beisner, B.E., Haydon, D.T., Cuddington, K., 2003. Alternative stable states in ecology. Front. Ecol. Environ. 1, 376–382.
Bolivar, M., Rivillas-Ospina, G., Fuentes, W., Guzman, A., Otero, L., Ruiz, G., Silva, R., Mendoza, E., Maza, M., Garcia, L., Berrio, Y., 2019. Anthropic Impact Assessment of Coastal Ecosystems in the Municipality of Puerto Colombia, NE Colombia. J. Coast. Res. 92, 112–120.
Bolla Pittaluga, M., Tambroni, N., Canestrelli, A., Slingerland, R., Lanzoni, S., Seminara, G., 2015. Where river and tide meet: The morphodynamic equilibrium of alluvial estuaries. J. Geophys. Res.-Earth Surf. 120, 75–94.
Bulleri, F., Chapman, M.G., 2010. The introduction of coastal infrastructure as a driver of change in marine environments. J. Appl. Ecol. 47, 26–35.
Carranza, M.L., Drius, M., Marzialetti, F., Malavasi, M., de Francesco, M.C., Acosta, A.T. R., Stanisci, A., 2020. Urban expansion depletes cultural ecosystem services: an insight into a Mediterranean coastline. Rendiconti Lincei-Scienze Fisiche E Naturali 31, 103–111.
Cooper, J.A.G., O'Connor, M.C., McIvor, S., 2020. Coastal defences versus coastal ecosystems: A regional appraisal. Mar. Policy 111, 2332.
Dai, Z.J., Liu, J.T., Xie, H.L., Shi, W.Y., 2014. Sedimentation in the Outer Hangzhou Bay, China: The Influence of Changjiang Sediment Load. J. Coast. Res. 30, 1218–1225.
Fan, Y.S., Chen, S.L., Zhao, B., Yu, S.B., Ji, H.Y., Jiang, C., 2018. Monitoring tidal flat dynamics affected by human activities along an eroded coast in the Yellow River Delta, China. Environ. Monit. Assess. 190, 1–17.
Fan, D.D., Tu, J.B., Shang, S., Cai, G.F., 2014. Characteristics of tidal-bore deposits and facies associations in the Qiantang Estuary, China. Mar. Geol. 348, 1–14.
Foley, M.M., Warrick, J.A., Ritchie, A., Stevens, A.W., Shafroth, P.B., Duda, J.J., Beirne, M.M., Paradis, R., Gelfenbaum, G., McCoy, R., Cubley, E.S., 2017. Coastal habitat and biological community response to dam removal on the Elwha River. Ecol. Monogr. 87, 552–577.
Golla, T.R., Pieterse, L., Jooste, C.M., Teske, P.R., 2020. Discovery of populations endemic to a marine biogeographical transition zone. Divers. Distrib. 26, 1825–1832.
Gong, J.X., 2002. Clarifying the standard deviational ellipse. Geogr. Anal. 34, 155–167.
Grases, A., Gracia, V., García-León, M., Lin-Ye, J., Sierra, J.P., 2020. Coastal Flooding and Erosion under a Changing Climate: Implications at a Low-Lying Coast (Ebro Delta). Water 12, 1–26.
Green, M.O., Coco, G., 2014. Review of wave-driven sediment resuspension and transport in estuaries. Rev. Geophys. 52, 77–117.
Hopper, S.D., Fiedler, P.L., Yates, C.J., 2021. Inselberg floristics exemplify the coast to inland OCBIL transition in a global biodiversity hotspot. Biol. J. Linn. Soc. 133, 624–644.
Hossain, M.S., Gain, A.K., Rogers, K.G., 2020. Sustainable coastal social-ecological systems: how do we define “coastal”? Int J Sust Dev World 27, 577–582.
Hou, Q., Lu, Y., Wang, Z., 2017. Cumulative impacts of high intensity reclamation in Bohai Bay on tidal wave system and its mechanism. Chin. Sci. Bull. 62, 3479–3489.
Hou, X.Y., Wu, T., Hou, W., Chen, Q., Wang, Y.D., Yu, L.J., 2016. Characteristics of coastline changes in mainland China since the early 1940s. Sci. China-Earth Sci. 59, 1791–1802.
Hu, T.A., Fan, J.J., Hou, H., Li, Y., Li, Y., Huang, K.N., 2021. Long-term monitoring and evaluation of land development in a reclamation area under rapid urbanization: A case-study in Qiantang New District, China. Land Degrad. Dev. 32, 3259–3271.
Hu, Y.K., Yu, Z.F., Zhou, B., Li, Y., Yin, S.J., He, X.Q., Peng, X.X., Shum, C.K., 2019. Tidal-driven variation of suspended sediment in Hangzhou Bay based on GOCI data. Int. J. Appl. Earth Obs. Geoinf. 82, 1–13.
Jia, J.J., Cai, T.L., Liu, Y.F., Chen, Y.N., Wang, X.K., Mei, Y.P., Shi, L.Q., 2019. A classification of coastline considering the impacts of human activities: remarks on latest practices on coastline survey in zhejiang province. Mar. Sci. 43, 13–23.
Koraim, A.S., Heikal, E.M., Zaid, A.A.A., 2014. Hydrodynamic characteristics of porous seawall protected by submerged breakwater. Appl. Ocean Res. 46, 1–14.
Kron, W., 2013. Coasts: the high-risk areas of the world. Nat. Hazards 66, 1363–1382.
Lefever, D.W., 1926. MEASURING GEOGRAPHIC CONCENTRATION BY MEANS OF THE STANDARD DEVIATIONAL ELLIPSE. Am. J. Sociol. 32, 88–94.
Li, J.T., Liu, Y.S., Yang, Y.Y., 2018. Land use change and effect analysis of tideland reclamation in Hangzhou Bay. J. Mt. Sci. 15, 394–405.
Liu, S., 2018. Land Institutional Reform and Structural Transformation in China: An Economic Interpretation for Chinas 40 Years Development Experience. China Land Sci. 32, 1–10.
Liu, K., Xue, Y., Chen, Z., Miao, Y., 2022. The spatiotemporal evolution and influencing factors of urban green innovation in China. Sci. Total Environ. 857, 159426.
Loder, N.M., Irish, J.L., Cialone, M.A., Wamsley, T.V., 2009. Sensitivity of hurricane surge to morphological parameters of coastal wetlands. Estuar. Coast. Shelf Sci. 84, 625–636.
Lonborg, C., Muller, M., Butler, E.C.V., Jiang, S., Ooi, S.K., Trinh, D.H., Wong, P.Y., Ali, S.M., Cui, C., Siong, W.B., Yando, E.S., Friess, D.A., Rosentreter, J.A., Eyre, B.D., Martin, P., 2021. Nutrient cycling in tropical and temperate coastal waters: Is latitude making a difference? Estuar. Coast. Shelf Sci. 262, 1–19.
Lovelock, C.E., Reef, R., 2020. Variable Impacts of Climate Change on Blue Carbon. One Earth 3, 195–211.

Lu, Y.H., Ma, Z.M., Zhang, L.W., Fu, B.J., Gao, G.Y., 2013. Redlines for the greening of China. Environ. Sci. Policy 33, 346–353.
Martinez, M.L., Silva, R., Lithgow, D., Mendoza, E., Flores, P., Martinez, R., Cruz, C., 2017. Human Impact on Coastal Resilience along the Coast of Veracruz, Mexico. J. Coast. Res. 143–153.
McLachlan, R.L., Ogston, A.S., Asp, N.E., Fricke, A.T., Nittrouer, C.A., Schettini, C.A.F., 2020. Morphological evolution of a macrotidal back-barrier environment: The Amazon Coast. Sedimentology 67, 3492–3512.
Moussa, R.M., Fogg, L., Bertucci, F., Calandra, M., Collin, A., Aubanel, A., Polti, S., Benet, A., Salvat, B., Galzin, R., Planes, S., Lecchini, D., 2019. Long-term coastline monitoring on a coral reef island (Moorea, French Polynesia). Ocean Coast. Manag. 180, 1–6.
Ni, Y.K., Chen, Y., 2022. Spatial-temporal distribution measurement of input-output efficiency of the water-energy-food nexus of the Yangtze River Economic Belt, China. Front. Ecol. Evol. 10.
Pan, C.H., Huang, W.R., 2010. Numerical Modeling of Suspended Sediment Transport Affected by Tidal Bore in Qiantang Estuary. J. Coast. Res. 26, 1123–1132.
Pan, C., Zheng, J., Cheng, G., He, C., Tang, Z., 2019. Spatial and temporal variations of tide characteristics in Hangzhou Bay and cause analysis. Ocean Eng. 37, 1–11.
Pereira, J., Ribeiro, P.A., Santos, A.M., Monteiro, C., Seabra, R., Lima, F.P., 2021. A comprehensive assessment of the intertidal biodiversity along the Portuguese coast in the early 2000s. Biodivers. Data J. 9.
PGGP, 2019. People's Government of Guangdong Province. http://www.gd.gov.cn/zwgk/wjk/zcfgk/content/post_2523845.html (accessed June 26. 2019).
Qiu, L.F., Zhang, M., Zhou, B.B., Cui, Y.Z., Yu, Z.L., Liu, T., Wu, S.H., 2021. Economic and ecological trade-offs of coastal reclamation in the Hangzhou Bay, China. Ecol. Indicat. 125.
Rietkerk, M., Bastiaansen, R., Banerjee, S., van de Koppel, J., Baudena, M., Doelman, A., 2021. Evasion of tipping in complex systems through spatial pattern formation. Science 374, 169-+.
Salmon, C., Duvat, V.K.E., 2018. Taking into account the natural coastal systems in coastal risk management. Houille Blanche-Revue Internationale De L Eau 104, 5–12.
Shao, Z.F., Ding, L., Li, D.R., Altan, O., Huq, M.E., Li, C.M., 2020. Exploring the Relationship between Urbanization and Ecological Environment Using Remote Sensing Images and Statistical Data: A Case Study in the Yangtze River Delta, China. Sustainability 12.
Singh, G.G., Sinner, J., Ellis, J., Kandlikar, M., Halpern, B.S., Satterfield, T., Chan, K.M. A., 2017. Mechanisms and risk of cumulative impacts to coastal ecosystem services: An expert elicitation approach. J. Environ. Manage. 199, 229–241.
Song, Z.K., Shi, W.Y., Zhang, J.B., Hu, H., Zhang, F., Xu, X.F., 2020. Transport Mechanism of Suspended Sediments and Migration Trends of Sediments in the Central Hangzhou Bay. Water 12.
Song, Y., Zhang, H., Hou, X., 2018. Shape changes of Bohai Sea since the early 1940s. J. Univers. Chin. Acad. Sci. 35, 761–770.
Su, F.Z., Gao, Y., Zhou, C.H., Yang, X.M., Fei, X.Y., 2011. Scale effects of the continental coastline of China. J. Geog. Sci. 21, 1101–1111.
Tak, W.J., Jun, K.W., Kim, S.D., Lee, H.J., 2020. Using Drone and LiDAR to Assess Coastal Erosion and Shoreline Change due to the Construction of Coastal Structures. J. Coast. Res. 674–678.
Thomas, C.G., Spearman, J.R., Turnbull, M.J., 2002. Historical morphological change in the Mersey Estuary. Cont. Shelf Res. 22, 1775–1794.
Tian, P., Li, J.L., Cao, L.D., Pu, R.L., Gong, H.B., Liu, Y.C., Zhang, H.T., Chen, H.L., 2021. Impacts of reclamation derived land use changes on ecosystem services in a typical gulf of eastern China: A case study of Hangzhou bay. Ecol. Ind. 132.
Tognin, D., D'Alpaos, A., Marani, M., Carniello, L., 2021. Marsh resilience to sea-level rise reduced by storm-surge barriers in the Venice Lagoon. Nat. Geosci. 14, 906–911.
USGS, 2018. Digital Shoreline Analysis System (DSAS). https://www.usgs.gov/centers/whcmsc/science/digital-shoreline-analysis-system-dsas (accessed October 4 2018).
Van der Wal, D., Pye, K., 2003. The use of historical bathymetric charts in a GIS to assess morphological change in estuaries. Geogr. J. 169, 21–31.
Wang, Y.H., Dong, P., Oguchi, T., Chen, S.L., Shen, H.T., 2013. Long-term (1842–2006) morphological change and equilibrium state of the Changjiang (Yangtze) Estuary, China. Cont. Shelf Res. 56, 71–81.
Wang, B.C., Eisma, D., 1990. Supply and deposition of sediment along the north bank of Hangzhou Bay. China. 25, 377–390.
Wang, H., Fan, W., Yun, C.X., 2004. Indicators and impact analysis of sediment from the Changjiang Estuary and East China Sea to the Hangzhou Bay. Acta Oceanol. Sin. 23, 297–308.
Wang, F., Pei, Y., Li, J., Shang, Z., Fan, C., Tian, L., Song, M., Geng, Y., Wang, H., 2010. Current elevation of Tianjin tidal zone and the urban safety of Binhai New Area, China. Geological Bulletin of China. Geol. Bull. China 29, 682–687.
Wang, B., Shi, W.Z., Miao, Z.L., 2015. Confidence Analysis of Standard Deviational Ellipse and Its Extension into Higher Dimensional Euclidean Space. PLoS One 10.
Wang, W., Wang, J., Choi, F.M.P., Ding, P., Li, X.X., Han, G.D., Ding, M.W., Guo, M.Q., Huang, X.W., Duan, W.X., Cheng, Z.Y., Chen, Z.Y., Hawkins, S.J., Jiang, Y.W., Helmuth, B., Dong, Y.W., 2020a. Global warming and artificial shorelines reshape seashore biogeography. Glob. Ecol. Biogeogr. 29, 220–231.
Wang, Z.F., Xu, X.M., Wang, H., Meng, S., 2020b. Does land reserve system improve quality of urbanization? Evidence from China. Habitat Int. 106, 2291.
Wang, J., Zhang, X.L., 2022. Land-based urbanization in China: Mismatched land development in the post-financial crisis era. Habitat Int. 125, 2598.
Ward, M.A., Hill, T.M., Souza, C., Filipczyk, T., Ricart, A.M., Merolla, S., Capece, L.R., O'Donnell, B.C., Elsmore, K., Oechel, W.C., Beheshti, K.M., 2021. Blue carbon stocks and exchanges along the California coast. Biogeosciences 18, 4717–4732.
Williams, B.A., Watson, J.E.M., Beyer, H.L., Klein, C.J., Montgomery, J., Runting, R.K., Roberson, L.A., Halpern, B.S., Grantham, H.S., Kuempel, C.D., Frazier, M., Venter, O., Wenger, A., 2022. Global rarity of intact coastal regions. Conserv. Biol.
Wu, F.L., 2022. Land financialisation and the financing of urban development in China. Land Use Policy 112, 4412.
Xie, D.F., Gao, S., Wang, Z.B., Pan, C.H., 2013. Numerical modeling of tidal currents, sediment transport and morphological evolution in Hangzhou Bay, China. Int. J. Sedim. Res. 28, 316–328.
Xie, D.F., Pan, C.H., Wu, X.G., Gao, S., Wang, Z.B., 2017. Local human activities overwhelm decreased sediment supply from the Changjiang River: Continued rapid accumulation in the Hangzhou Bay-Qiantang Estuary system. Mar. Geol. 392, 66–77.
Xu, Y., Cai, Y.P., Sun, T., Yin, X.A., Tan, Q., 2017. Development of an integrated indicator system to assess the impacts of reclamation engineering on a river estuary. Mar. Pollut. Bull. 119, 50–59.
Xu, H., Zhang, Y., Hou, X., Li, D., 2022. Morphological changes of major gulfs along the coast of China from 2010 to 2020. J. Nat. Resour. 37, 1010–1024.
Yi, L., Chen, J.S., Jin, Z.F., Quan, Y.M., Han, P.P., Guan, S.J., Jiang, X.L., 2018. Impacts of human activities on coastal ecological environment during the rapid urbanization process in Shenzhen, China. Ocean Coast. Manag. 154, 121–132.
Yuan, F., Wei, Y.D., Xiao, W.Y., 2019. Land marketization, fiscal decentralization, and the dynamics of urban land prices in transitional China. Land Use Policy 89, 4208.
Zhang, W., Xu, Y., Hoitink, A.J.F., Sassi, M.G., Zheng, J.H., Chen, X.W., Zhang, C., 2015. Morphological change in the Pearl River Delta, China. Mar. Geol. 363, 202–219.
Zhou, Y., Ning, L., Bai, X., 2018. Spatial and temporal changes of human disturbances and their effects on landscape patterns in the Jiangsu coastal zone, China. Ecol. Ind. 93, 111–122.
Zhu, L.H., Wu, J.Z., Xu, Z.Q., Xu, Y.C., Lin, J., Hu, R.J., 2014. Coastline movement and change along the Bohai Sea from 1987 to 2012. J. Appl. Remote Sens. 8.